applied sciences

MDPI

Article

Design, Synthesis and Evaluation of Novel Pyrrolidinone-Based ACE2 Inhibitors: Preliminary Study

Ilaria Nigro [1], Maria Francesca Armentano [1], Anna Caruso [2,3,*], Hussein El-Kashef [4,5], Federica Giuzio [6], Antonio Vassallo [1], Francesca Finelli [3,7], Magnus Monné [1] and Carmela Saturnino [1,3]

[1] Department of Health Sciences, University of Basilicata, 85100 Potenza, Italy; ilaria.nigro@unibas.it (I.N.); mariafrancesca.armentano@unibas.it (M.F.A.); antonio.vassallo@unibas.it (A.V.); magnus.monne@unibas.it (M.M.); carmela.saturnino@unibas.it (C.S.)
[2] Department of Basic and Applied Sciences, University of Basilicata, 85100 Potenza, Italy
[3] UNIPOSM (Università Popolare Nuova Scuola Medica Salernitana)—Scuola di Nutraceutica, 84123 Salerno, Italy; medfinelli@gmail.com
[4] Faculty of Science, Assiut University, Assiut 71516, Egypt; elkashef@aun.edu.eg
[5] Faculty of Pharmacy, Sphinx University, New Assiut 71515, Egypt
[6] U.O.C. (Unità Operativa Complessa) Primary Care and Territorial Health, Social and Health Department, State Hospital, 47893 San Marino, San Marino; federica.giuzio@gmail.com
[7] Struttura Complessa U.O.C. Pediatria Azienda Ospedaliera S. Giuseppe Moscati, 83100 Avellino, Italy
* Correspondence: anna.caruso@unibas.it

Abstract

This study focuses on the rational design and synthesis of new pyrrolidinone derivatives aimed at inhibiting the ACE2 receptor, a key entry point for SARS-CoV-2. Building on structural insights from known inhibitors like MLN-4760, five compounds featuring a pyrrolidinone core, with some incorporating indole rings, were synthesized and characterized. Their inhibitory activity against ACE2 was evaluated *in vitro*, with compound **4** showing the most promising results, further confirmed through cytotoxicity assays and molecular docking studies. Docking analysis revealed favorable binding interactions within the ACE2 active site, supporting the potential of compound **4** as a therapeutic agent. These findings provide a foundation for future *in vivo* studies and highlight the potential development of novel therapeutics targeting ACE2-related diseases, including COVID-19.

Keywords: SARS-CoV-2; ACE2; TMPyP4; ACE2 inhibitors; MLN-4760; pyrrolidinone derivatives

Academic Editor: Burkhard Poeggeler

Received: 22 December 2025
Revised: 4 February 2026
Accepted: 6 February 2026
Published: 9 February 2026

1. Introduction

SARS-CoV-2, responsible for coronavirus disease 19 (COVID-19), is an RNA virus belonging to the coronavirus (CoV) family [1,2]. Under the electron microscope, it appears like a crown (hence the name corona virus), a property given by the presence on the external envelope of spike (S) glycoproteins, which are responsible for entry into the human host cells. The S-protein consists of two subunits, S1 and S2; S1 has the receptor-binding domain (RBD), while the S2 subunit is responsible for viral membrane fusion. Entry into host cells depends on the binding between the S1 subunit and a cellular receptor which facilitates the attachment of the virus to the surface of the target cells. In particular, it has been demonstrated that the virus uses angiotensin-converting enzyme 2 (ACE2) as an entry receptor and transmembrane serine protease 2 (TMPRSS2) for the activation of the S

protein [3]. ACE2 is a Zn^{2+} and chloride-dependent metallopeptidase, which is expressed in blood vessel endothelial cells of various organs, but especially in the lung, and is involved in the metabolism of important biologically active peptides, such as angiotensin I and bradykinin [4]. In particular, it catalyzes the transformation of angiotensin I into angiotensin II, thus intervening in the regulation of the renin–angiotensin–aldosterone system (RAAS). Angiotensin II is a powerful vasoconstrictor that stimulates peripheral vascular resistance and an increase in blood pressure, but it is also involved in the secretion of aldosterone with a consequent increase in cardiac output. It is worth noting, that there is also another isoform of ACE, ACE1 [5], but only ACE2 represents an entry gate for viruses of the coronavirus family, such as SARS-CoV-2. It has been hypothesized that a greater expression of ACE2 in the lung leads to an exacerbation of the respiratory symptoms of SARS-CoV-2 infection [6]. Angiotensin-converting enzyme 2 (ACE2) plays a pivotal regulatory role in both cardiovascular physiology and pathological angiogenesis. By counterbalancing angiotensin II signaling, ACE2 modulates endothelial cell migration and vascular tube formation, thereby influencing angiogenic processes. Accumulating evidence demonstrates that ACE2 exerts antitumor effects by suppressing VEGF-mediated angiogenesis and inhibiting tumor cell invasion, particularly through regulation of the VEGFA/VEGFR2/ERK signaling pathway. Overall, these findings highlight ACE2 as a critical modulator of vascular homeostasis and tumor-associated angiogenesis [7–10].

In the most serious cases, SARS-CoV-2 infection can cause acute inflammation and interstitial pneumonia, where there is a reduction in gas exchange in the alveoli. In conditions of acute hypoxia, free radicals (ROS) are formed that generate an inflammatory state due to a reduction in oxygen supply through alteration of the vessel wall starting from endothelium/cardiac alteration [11,12]. Furthermore, after entry into the cell through ACE2 receptor binding and internalization, SARS-CoV-2 forces the host cells to produce proteins useful for its replication and viral particle assembly. These intracellular processes are the underlying basis for strong inflammation, ROS production, and alterations in the functionality of the pulmonary alveoli and the structure of the vessels, which leads to edema. This is the reason why forced oxygen ventilation becomes necessary to remove the hypoxic state. Therefore, by reducing the inflammatory state it is possible to avoid acute respiratory crises [13].

Among the various studies on drugs to be used in SARS-CoV-2 infection, we recall that G-quadruplex specific ligands, namely porphyrin-tetra-tosylsulfonates 4,4′,4″,4‴-(porphyrin-5,10,15,20-tetrayl)tetrakis(1-methylpyridin-1-ium) tetratosylate (TMPyP4) (**I**) (Figure 1), showed better antiviral effects than remdesivir on Vero E6 cells, Syrian hamster and the human ACE2 transgenic mouse model of SARS-CoV-2 infection, with no significant toxicity [14]. Most importantly, this study provided an alternative strategy for COVID-19 treatment by targeting the secondary genomic structures of SARS-CoV-2, paving the way to the rational design and synthesis of new and safer agents.

https://doi.org/10.3390/app16041718

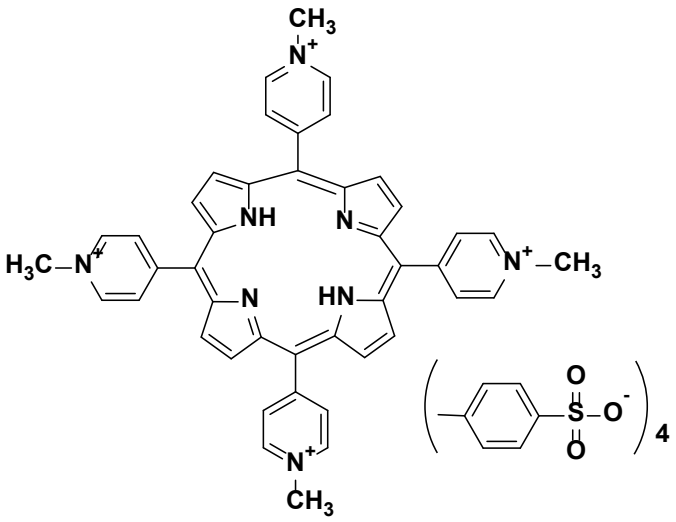

Figure 1. Structure of 4,4′,4″,4‴-(porphyrin-5,10,15,20-tetrayl)tetrakis(1-methylpyridin-1-ium) tetratosylate (TMPyP4) (**I**).

Our current study was directed towards a different approach: the design of novel selective ACE2 inhibitors with potential therapeutic applications for ACE2-associated diseases including COVID-19. To optimize interactions with the ACE2 catalytic site, we pursued the synthesis of some molecules characterized by reduced size and increased flexibility compared with TMPyP4 (**I**). These compounds were specifically tailored to engage with the ACE2 binding pocket in the conformation inhibited by MLN-4760 (**II**) (Figure 2), a selective ACE2 inhibitor [15].

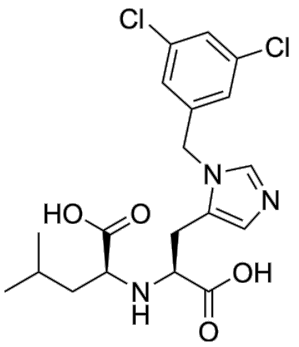

Figure 2. Structure of MLN-4760 (**II**).

Our design efforts focused on five pyrrolidinones (Figure 3), which we synthesized, tested, and correlated to the structure of MLN-4760 (**II**). A key consideration was the inclusion of at least one nitrogen heterocyclic ring, a feature shared with both MLN-4760 (**II**) and a related compound (**I**). The structure of all five compounds (**1–5**, Figure 3) contain a pyrrolidinone core. Additionally, compounds **4** and **5** incorporate an indole ring, a scaffold known for its diverse other therapeutic activities, including anti-inflammatory, antimicrobial, antioxidant, antitumor, and antiviral properties [16–22]. Moreover, recent research further emphasizes the significance of the indole core in potential drug candidates for SARS-CoV-2 [23,24]. Consistent with MLN-4760 (**II**), our molecules also feature polar functional groups, such as the amide in compounds **2–5**, which are crucial for interactions within the ACE2 pocket.

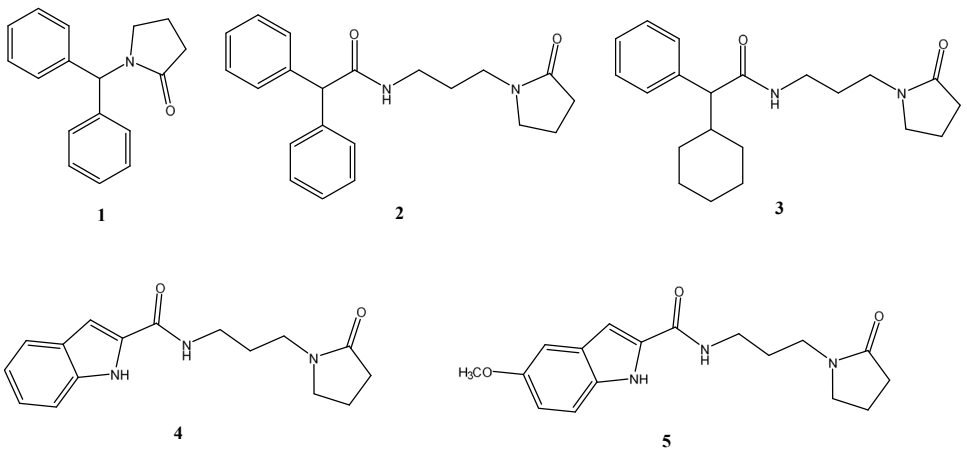

Figure 3. Structure of pyrrolidinones (**1–5**).

2. Materials and Methods

2.1. Chemistry

Commercial reagents were purchased from Aldrich (Milano, Italy), Acros Organics (Geel, Belgium) and Alfa Aesar (London, UK) and used without additional purification. Melting points were determined on a Kofler melting point apparatus. Mass spectra were taken on a JEOL JMS GCMate spectrometer (JEOL, Tokyo, Japan) at an ionizing potential of 70 eV (EI). ^{1}H-NMR (300 MHz) and ^{13}C-NMR (75 MHz) were recorded on a Bruker Avance 300 MHz spectrometer (Bruker, Billerica, MA, USA). Chemical shifts were expressed in parts per million downfield from tetramethylsilane as an internal standard. The progress of the reactions and the purity of the synthesized products were monitored by thin layer chromatography (TLC), using aluminum plates covered with Whatman K6F silica gel (or Merck-25 DC-Alufolien Kiesegel 60 F254) and alumina (Merck, Milano, Italy) with fluorescence indicators, using the appropriate eluents and observed under ultraviolet light (254 nm). As solid supports for liquid chromatography adsorption, Silica Gel 60 (Merck), Alumina 90 (Merck) and celite 545 were employed.

2.2. General Procedure for the Synthesis of Compounds ***7***, ***9a***, ***9b***, ***11a***, ***11b***

A mixture of amine **6** or *N*-(3-aminopropyl)alkylamides **8a, 8b, 10a, 10b** (1.0 mmol), 4-chlorobutyryl chloride (1.5 mmol), Na_2CO_3 (3.0 mmol) in toluene (20 mL) was heated at 110 °C under stirring for 5 h. The reaction mixture was then allowed to cool to room temperature and diluted with ice-cold water (30 mL). The resulting mixture was extracted with dichloromethane (3 × 30 mL). The combined organic layer was washed with brine, dried over anhydrous Na_2SO_4 and concentrated under vacuum. The residue obtained was chromatographed on silica gel column using n-hexane/diethyl ether (1:2) as an eluent to give the desired derivatives **7, 9a, 9b, 11a, 11b** (yield 65–80%).

2.2.1. *N*-Benzhydryl-4-Chlorobutanamide (**7**)

White solid. ^{1}H-NMR (300 MHz, $CDCl_3$): δ = 8.14 (br, 1H, N*H*), 7.42–7.34 (m, 8H, Ar), 7.24–7.10 (m, 2H, Ar), 6.20 (s, 1H, *CH*), 3.70–3.60 (m, 2H, *CH*$_2$Cl), 2.36–2.31 (m, 2H, COC*H*$_2$), 1.92–1.85 (m, 2H, *CH*$_2$); MS (EI) *m*/*z* (%): 289 [M$^+$, 2].

2.2.2. 4-Chloro-*N*-(3-(2,2-Diphenylacetamido)propyl)butanamide (**9a**)

White solid. ^{1}H-NMR (300 MHz, $CDCl_3$): δ = 8.01 (br, 1H, N*H*), 7.73 (br, 1H, N*H*), 7.41–7.29 (m, 6H, Ar), 7.23–7.20 (m, 4H, Ar), 5.10 (s, 1H, C*H*), 3.70–3.65 (m, 2H, C*H*$_2$Cl), 3.44–3.40 (m, 4H, HNC*H*$_2$ CH$_2$C*H*$_2$NH), 2.37–2.33 (m, 2H, COC*H*$_2$), 1.90–1.83 (m, 4H, CH$_2$C*H*$_2$CH$_2$, C*H*$_2$CH$_2$Cl); MS (EI) *m*/*z* (%): 374 [M$^+$, 2].

2.2.3. 4-Chloro-*N*-(3-(2-Cyclohexyl-2-Phenylacetamido)propyl)butanamide (**9b**)

White solid. ^{1}H-NMR (300 MHz, $CDCl_3$): δ = 8.01 (br, 1H, N*H*), 7.72 (br, 1H, N*H*), 7.37–7.29 (m, 5H, Ar), 3.50 (d, 1H, C*H*), 3.70–3.65 (m, 2H, CH_2Cl), 3.43–3.19 (m, 4H, HNCH_2CH_2CH_2NH), 2.36–2.32 (m, 2H, COCH_2), 2.13–2.10 (m, 1H, C*H*), 1.91–1.83 (m, 4H, CH_2CH_2CH_2, CH_2CH_2Cl), 1.64–1.36 (m, 10H, 5CH_2); MS (EI) *m*/*z* (%): 380 [M$^+$, 2].

2.2.4. *N*-(3-(4-Chlorobutanamido)propyl)-1*H*-Indole-2-Carboxamide (**11a**)

White solid. ^{1}H-NMR (300 MHz, $CDCl_3$): δ = 11.55 (br, 1H, N*H*), 9.00 (br, 1H, N*H*), 7.70 (br, 1H, N*H*), 7.59–7.55 (m, 1H, Ar), 7.52–7.50 (m, 1H, Ar), 7.40 (s, 1H, Ar), 7.30–7.29 (m, 2H, Ar), 3.70–3.66 (m, 2H, CH_2Cl), 3.41–3.21 (m, 4H, HNCH_2CH_2CH_2NH), 2.36–2.33 (m, 2H, COCH_2), 1.88–1.82 (m, 4H, CH_2CH_2CH_2, CH_2CH_2Cl); MS (EI) *m*/*z* (%): 323 [M$^+$, 2].

2.2.5. *N*-(3-(4-Chlorobutanamido)propyl)-5-Methoxy-1*H*-Indole-2-Carboxamide (**11b**)

White solid. ^{1}H-NMR (300 MHz, $CDCl_3$): δ = 11.55 (br, 1H, N*H*), 9.01 (br, 1H, N*H*), 7.72 (br, 1H, N*H*), 7.60–7.55 (d, 1H, Ar), 7.48–7.45 (d, 1H, Ar), 7.39–7.37 (d, 1H, Ar), 6.81–6.78 (d, 1H, Ar), 3.80 (s, 3H, OCH_3), 3.71–3.66 (m, 2H, CH_2Cl), 3.42–3.20 (m, 4H, HNCH_2CH_2CH_2NH), 2.37–2.33 (m, 2H, COCH_2), 1.90–1.84 (m, 4H, CH_2CH_2CH_2, CH_2CH_2Cl); MS (EI) *m*/*z* (%): 353 [M$^+$, 2].

*2.3. General Procedure for the Synthesis of Compounds **1**–**5***

A mixture of the amido derivative (**7, 9a, 9b, 11a or 11b**) (1.0 mmol) and Na_2CO_3 (1.5 mmol) in DMF (20 mL) was heated at 150 °C under stirring for 12 h. Water (50 mL) was then added, and the resulting mixture was extracted with ethyl acetate (3 × 20 mL). The combined organic layer was washed with brine, dried over anhydrous Na_2SO_4, and concentrated under vacuum. The residue obtained was chromatographed on silica gel column using petroleum ether/EtOAc (1:1) as an eluent to give the desired pyrrolidinones **1**–**5** (yield 60–72%).

2.3.1. 1-Benzhydrylpyrrolidin-2-one (**1**)

White solid, mp: 131–133 °C. ^{1}H-NMR (300 MHz, $CDCl_3$): δ = 7.48–7.27 (m, 4H, Ar), 7.24–7.09 (m, 6H, Ar), 6.20 (s, 1H, C*H*), 3.40–3.31 (m, 2H, NCH_2), 2.41–2.30 (m, 2H, COCH_2), 2.10–1.95 (m, 2H, CH_2); ^{13}C-NMR (75 MHz, $CDCl_3$): δ =174.19, 138.26, 130.14, 128.91, 126.15, 72.46, 46.61, 31.17, 19.26; MS (EI) *m*/*z* (%): 252 [M$^+$, 1]; Anal. calcd for $C_{17}H_{17}NO$: C 81.24, H 6.82, N 5.57, found: C 81.26, H 6.81, N 5.55.

2.3.2. *N*-(3-(2-Oxopyrrolidin-1-yl)propyl)-2,2-Diphenylacetamide (**2**)

White solid, mp: 116–118 °C. ^{1}H-NMR (300 MHz, $CDCl_3$): δ = 8.03 (br, 1H, NH), 7.40–7.30 (m, 6H, Ar), 7.22–7.19 (m, 4H, Ar), 5.20 (s, 1H, C*H*), 3.43–3.39 (m, 2H, HNCH_2), 3.33–3.28 (m, 2H, NCH_2 pyrrolidinone), 3.20–3.16 (m, 2H, NCH_2), 2.35–2.30 (m, 2H, COCH_2), 2.11–1.98 (m, 2H, CH_2CH_2CO), 1.90–1.87 (m, 2H, CH_2); ^{13}C-NMR (75 MHz, $CDCl_3$): δ =174.99, 170.96, 138.54, 129.21, 128.25, 126.22, 58.36, 50.71, 47.97, 38.06, 31.05, 26.56, 17.76; MS (EI) *m*/*z* (%): 337 [M$^+$, 1]; Anal. calcd for $C_{21}H_{24}N_2O_2$: C 74.97, H 7.19, N 8.33, found: C 74.99, H 7.20, N 8.31.

2.3.3. 2-Cyclohexyl-*N*-(3-(2-Oxopyrrolidin-1-yl)propyl)-2-Phenylacetamide (**3**)

White solid, mp: 101–103 °C. ^{1}H-NMR (300 MHz, $CDCl_3$): δ = 8.02 (br, 1H, N*H*), 7.36–7.28 (m, 5H, Ar), 3.60 (d, 1H, C*H*), 3.33–3.30 (m, 2H, NCH_2 pyrrolidinone), 3.28–3.18 (m, 4H, HNCH_2, CH_2N), 2.34–2.31 (m, 2H, COCH_2), 2.14–2.11 (m, 1H, C*H*), 2.10–1.97 (m, 2H, CH_2CH2CO), 1.64–1.37 (m, 10H, 5CH_2) 1.90–1.87 (m, 2H, HNCH$_2$CH_2CH$_2$N); ^{13}C-NMR (75 MHz, $CDCl_3$): δ =174.92, 170.46, 139.84, 128.11, 125.95, 50.76, 48.51, 47.96, 38.02, 32.55,

31.09, 30.08, 26.51, 26.09, 25.43, 17.72; MS (EI) *m*/*z* (%): 343 [M⁺, 1]; Anal. calcd for $C_{21}H_{30}N_2O_2$: C 73.65, H 8.83, N 8.18, found: C 73.67, H 8.81, N 8.20.

2.3.4. *N*-(3-(2-Oxopyrrolidin-1-yl)propyl)-1*H*-Indole-2-Carboxamide (**4**)

Yellow solid, mp: 224–226 °C. ^{1}H-NMR (300 MHz, $CDCl_3$): δ = 11.55 (br, 1H, N*H*), 8.99 (br, 1H, CON*H*), 7.63–7.60 (m, 1H, Ar), 7.55–7.52 (m, 1H, Ar), 7.40 (d, 1H, Ar), 7.01–6.98 (m, 2H, Ar), 3.32–3.30 (m, 2H, NCH_2 pyrrolidinone), 3.26–3.19 (m, 4H, HNCH_2, CH_2N), 2.33–2.30 (m, 2H, COCH_2), 2.00–1.98 (m, 2H, CH_2) 1.90–1.87 (m, 2H, HNCH$_2$CH_2CH$_2$N); ^{13}C-NMR (75 MHz, $CDCl_3$): δ =174.93, 160.34, 139.00, 138.54, 131.31, 122.07, 120.95, 119.32, 114.98, 111.10, 50.79, 47.91, 39.86, 31.08, 26.55, 17.79; MS (EI) *m*/*z* (%): 286 [M⁺, 1]; Anal. calcd for $C_{16}H_{19}N_3O_2$: C 67.35, H 6.71, N 14.73, found: C 67.33, H 6.70, N 14.74.

2.3.5. 5-Methoxy-*N*-(3-(2-Oxopyrrolidin-1-yl)propyl)-1*H*-Indole-2-Carboxamide (**5**)

Yellow solid, mp: 199–201 °C. ^{1}H-NMR (300 MHz, $CDCl_3$): δ = 11.52 (br, 1H, N*H*), 9.02 (br, 1H, CON*H*), 7.60 (d, 1H, Ar), 7.45 (d, 1H, Ar), 7.40 (d, 1H, Ar), 6.98 (d, 1H, Ar), 3.80 (s, 3H, OCH_3), 3.33–3.30 (m, 2H, NCH_2 pyrrolidinone), 3.27–3.18 (m, 4H, HNCH_2, CH_2N), 2.34–2.31 (m, 2H, COCH_2), 2.00–1.97 (m, 2H, CH_2) 1.90–1.87 (m, 2H, HNCH$_2$CH_2CH$_2$N); ^{13}C-NMR (75 MHz, $CDCl_3$): δ =174.90, 160.54, 154.41, 138.24, 132.11, 132.07, 114.95, 112.32, 112.12, 111.32, 56.03, 50.72, 47.91, 39.96, 31.02, 26.55, 17.70; MS (EI) *m*/*z* (%): 316 [M⁺, 1]; Anal. calcd for $C_{17}H_{21}N_3O_3$: C 64.74, H 6.71, N 13.32, found: C 64.72, H 6.69, N 13.34.

2.4. Biology

Dulbecco's modified Eagle's medium/nutrient mixture F-12 (1:1) (DMEM/F12-HEPES) medium and Dulbecco's modification of Eagle's medium (DMEM) were purchased from Corning (Corning, NY, USA). Dulbecco's phosphate-buffered saline solution (DPBS), L–glutamine, penicillin–streptomycin solution and fetal bovine serum (FBS) were obtained from EuroClone (Milan, Italy). Dimethyl sulfoxide (DMSO), trypsin–EDTA solution, fibronectin, gelatin from bovine skin, Claycomb medium, norepinephrine and thiazolyl blue tetrazolium bromide (MTT), were purchased from Sigma Aldrich-Merck (Saint Louis, MO, USA).

2.5. Angiotensin II Converting Enzyme (ACE2) Inhibition Screening Studies

Stock solutions (10 mM) of compounds **1–5** in DMSO were prepared. ACE2 activity was measured using angiotensin II converting enzyme (ACE2) inhibitor screening kit (cat. No. MAK378, Sigma Aldrich, St. Louis, MO, USA). The assay was performed in triplicate, using an aliquot of 10 µL from each sample and following the manufacturer's protocol. The inhibitory activity of all the five compounds was evaluated at a final concentration of 1 µM. Fluorescence was read using a VICTOR Nivo multimode microplate reader (PerkinElmer). Two time points were chosen (T1 = 105 s and T2 = 370 s, in the linear range of the graph) and the corresponding fluorescence values were obtained (RFU1 and RFU2, RFU = relative fluorescence unit). The slopes were therefore calculated for all the samples, and it was possible to calculate the % relative inhibition of each molecule using the formula:

$$\%\boldsymbol{RelativeInhibition} = (\boldsymbol{SlopeEC} - \boldsymbol{SlopeS}/\boldsymbol{SlopeEC}) * \mathbf{100}$$

(EC = enzyme control (ACE2, no inhibition), S = sample (ACE2 + molecule)

2.6. Cell Lines and Culture Conditions

The immortalized neuroblastoma cell line SH-SY5Y was maintained in DMEM/F-12-HEPES medium supplemented with 10% fetal bovine serum (FBS), 100 U/mL penicillin, and 100 µg/mL streptomycin. Human embryonic kidney (HEK293) cells were cultured in DMEM supplemented with 10% FBS, 2 mM L-glutamine, 100 U/mL penicillin, and 100

μg/mL streptomycin. HL-1 cardiomyocytes were grown in gelatin/fibronectin-coated flasks using Claycomb medium supplemented with 10% FBS, 100 U/mL penicillin, 100 μg/mL streptomycin, 2 mM L-glutamine, and 0.1 mM norepinephrine [(±)-Arterenol]. Caco2 colorectal adenocarcinoma cells were cultured in high-glucose (4.5 g/L) DMEM supplemented with 10% FBS, 2 mM L-glutamine, 100 U/mL penicillin, and 100 μg/mL streptomycin. All cell cultures were maintained at 37 °C in a humidified atmosphere with 5% CO_2 and passaged every 48 h.

Compound **4** was dissolved in dimethyl sulfoxide (DMSO) as 50 mM stock solutions and stored at 4 °C until use. The working solutions were freshly prepared, diluting in cell culture medium. The final concentration of DMSO was always within the limit of 0.8% (v/v), which did not affect cell growth when compared with the vehicle-free controls.

2.7. Measurement of Cell Viability

Cytotoxicity of the synthetic molecules was assessed by MTT [3-(4,5-dimethylthiazol-2-yl)-2,5-diphenyltetrazolium bromide] colorimetric assay. Experimentally, SH-SY5Y, HEK239, HL-1, and Caco-2 cells were seeded in 96-well plates (2 × 104 cells per well) and incubated for 24 h. The cells were treated with different concentrations of the compound (40μM, 20μM, 10μM, 5μM, 1μM, 0.5μM and 0.1 μM) for 24 h. As a negative control, cells were treated with DMSO at the highest concentration used in the treatments. Thereafter, the media were discarded and the cells were incubated with 100 μL of 0.75 mg/mL MTT solution for 4 h in the dark at 37 °C. Subsequently, formazan crystals were dissolved by the addition of 100 μL/well 1:1 DMSO:isopropanol. Absorbance was measured using a Multiskan Go spectrophotometer (Thermo Scientific, Waltham, MA, USA) at a wavelength of 570 nm with background subtraction at 630 nm. The 50% inhibitory concentration (IC_{50}) was calculated using GraphPad Prism software V. 8.4.2 (GraphPad, La Jolla, CA, USA).

2.8. Molecular Docking

The docking studies used the X-ray structure of human ACE2 inhibited by MLN-4760 (PDB ID 1R4L) with 3.0 Å resolution [25]. The protein structure (with MLN-4760 removed) and the ligands were prepared with AutoDockTools 1.5.7 of the MGLTool package 1.5.7. The ligands were prepared with Gasteiger charges, merged non-polar hydrogens, aromatic carbons and rotatable bonds. In silico molecular docking of conformationally flexible compounds into the semi-rigid structure of acetylcholinesterase was performed with the Lamarckian genetic algorithm in AutoDock Vina 1.1.2 [26]. Selected flexible residues were E145, W271, R273, V243, H345, P346, T347, K363, D367, D368, E375, E406, F504, H505, Y510, R514 and Y515. Grid box size was 24 Å × 24 Å × 28 Å centered at the coordinates (41,4,29) and the exhaustiveness 20. The docking solutions were ranked by the binding site scoring function of AutoDock Vina, which estimates the binding energy (affinity), without any rescoring/re-ranking.

3. Results and Discussion

SARS-CoV-2 is a member of the coronavirus (CoV) family and it is the causative agent of COVID-19 [27]. This infection often leads to severe inflammation of the respiratory tract epithelium and can result in patient mortality. Currently, there are no definitive drug therapies. The presence of spike (S) glycoproteins on its outer envelope facilitates its entry into target cells [28]. The S1 subunit of protein S engages ACE2 on the surface of the target cells as an entry receptor and the serine protease TMPRSS2 for the activation of protein S [29]. The ACE2 receptor is an important protein that regulates the vasoconstriction processes of the arteries of the lungs, protecting them from damage that can be caused by infections and inflammation. In severe cases, SARS-CoV-2 infection may trigger

acute inflammation in lung tissues giving rise to interstitial pneumonia and significantly impairing gas exchange in the alveoli [30].

Several reports [31–34] have shown that the binding affinity of SARS-CoV-2 for the ACE2 receptor via the spike receptor-binding domain (S-RBD) is nearly tenfold higher than that observed for the SARS-CoV RBD. This suggests that ACE2 represents the primary, and maybe the only, receptor responsible for viral attachment to the host cell membrane. Therefore, the possible therapeutic targets for treating COVID-19 are the SARS-CoV-2/ACE2 interactions, either directly by interfering with the surfaces involved in the interaction or indirectly by modifying the conformations of RBD or ACE2, which in the latter case might affect binding, internalization or the regulation of its expression. To date, some compounds have been reported as inhibitors of ACE2, such as MLN-4760 (**II**, Figure 2) [35], whereas others, for example the well-established anti-influenza drug Arbidol (Umifenovir **III**, Figure 4), interfere with the SARS-CoV-2 RBD–ACE2 interaction [36].

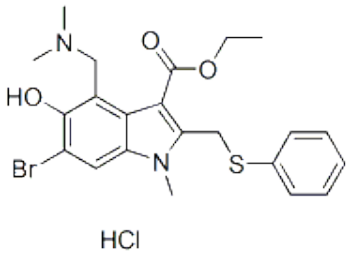

Figure 4. Structure of Arbidol (III).

In this preliminary study, we have investigated the ACE2 inhibitory effects of compounds **1–5**, of which some are structurally related to both MLN-4760 and Arbidol. The most active derivative, indole **4**, was selected for further cytotoxicity studies on uninfected human cells and a molecular docking analysis.

3.1. Chemistry

Pyrrolidinone derivatives **1–5** were synthesized as described in Schemes 1–3. Specifically, diphenylmethanamine (**6**) or *N*-(3-aminopropyl)acrylamide (**8a, 8b, 10a, 10b**) (molecules present in our chemistry library) were reacted with 4-chlorobutyryl chloride in toluene under reflux in the presence of sodium carbonate. The amido derivatives (**7, 9a, 9b, 11a, 11b**) obtained were cyclized in a basic medium, by heating under reflux in the higher boiling point, *N*,*N*-dimethylformamide (DMF) in the presence of sodium carbonate.

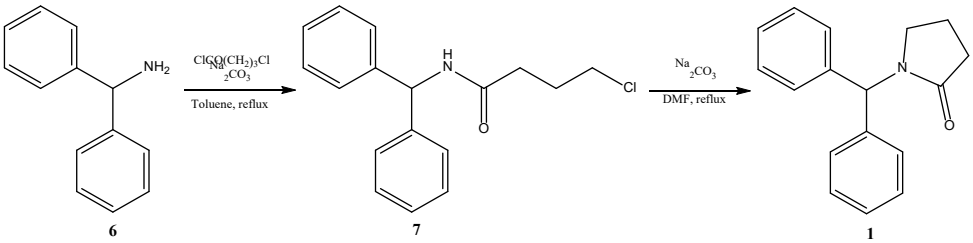

Scheme 1. Synthetic route for 1-benzhydrylpyrrolidin-2-one (**1**).

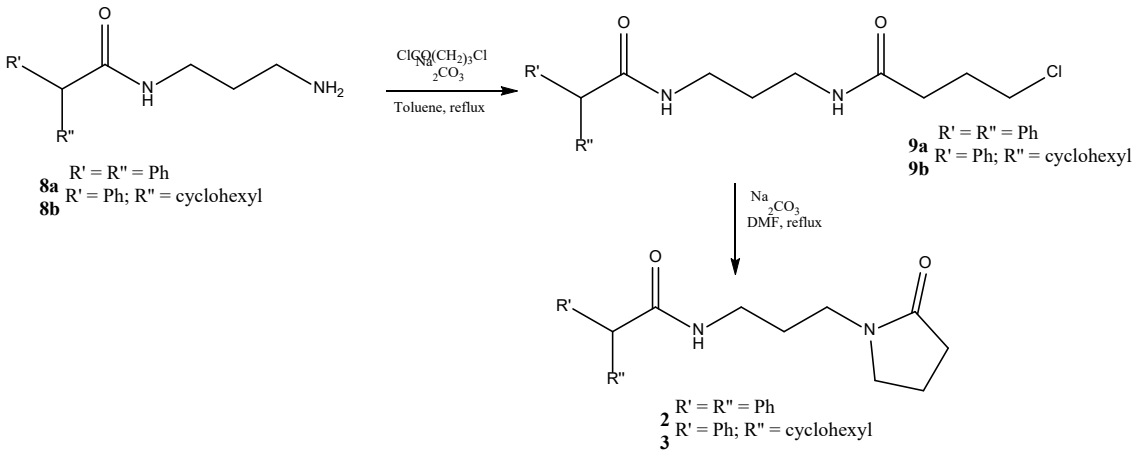

Scheme 2. Synthetic route for compounds **2** and **3**.

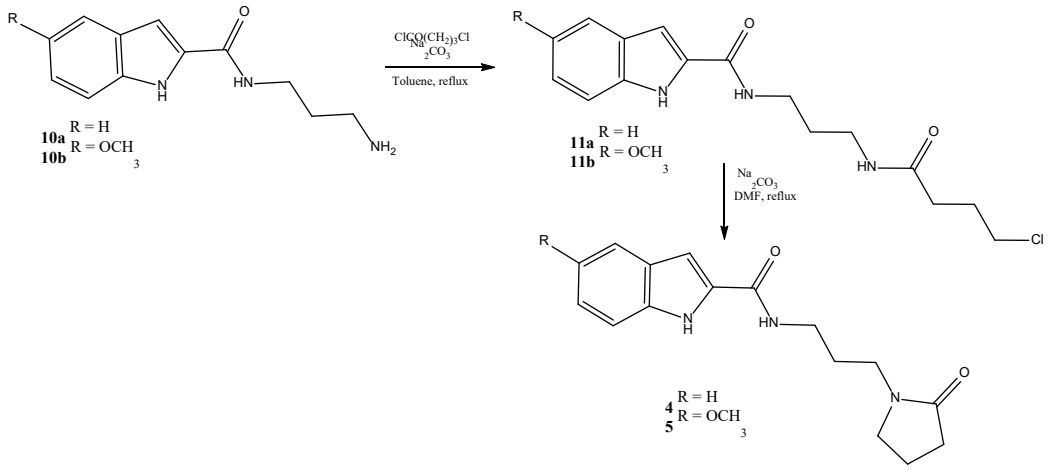

Scheme 3. Synthetic route for compounds **4** and **5**.

3.2. Angiotensin II Converting Enzyme (ACE2) Inhibition Studies

Compounds **1–5** were studied for their ACE2 inhibitory activity. The stock solutions of all the molecules (**1–5**) were prepared by dissolving these compounds in DMSO, thus obtaining a starting concentration of 10 mM for each compound. ACE2 activity was measured using the angiotensin II converting enzyme (ACE2) inhibitor screening kit (cat. No. MAK378, Sigma Aldrich, St. Louis, MO, USA). The assay was performed in triplicate, using an aliquot of 10 µL from each sample and following the manufacturer's protocol. The inhibitory activity of all five molecules was evaluated at a final concentration of 1 µM. Fluorescence was read using a VICTOR Nivo multimode microplate reader (PerkinElmer). The % relative inhibition of each molecule determined at the concentration of 1 µM are reported in the tables below (Table 1). The compound with the greatest inhibitory action on the ACE2 receptor is **4**.

Table 1. Inhibitory activity of compounds **1–5** against ACE2 at a concentration of 1 µM, negative control (CTRL) [a].

SAMPLE (1 µM)	% Inhibition
ACE2 (CTRL)	0
ACE2 + Commercial Inhibitor	98.66 ± 2.02
ACE2 + **1**	0
ACE2 + **2**	20.62 ± 0.09
ACE2 + **3**	0

ACE2 + **4**	25.14 ± 0.11
ACE2 + **5**	1.07± 0.12

[a] Each analysis was performed in triplicate. Values are means ± SD.

3.3. Cytotoxicity Studies

To exclude a potential cytotoxic effect of compound **4**, it was tested on different cell lines using a concentration range of 0.1, 0.5, 1, 5, 10, 20, and 40 μM. This range was selected based on previous *in vitro* data showing that compound **4** is able to inhibit the ACE2 enzyme at a concentration of 10 μM. The cell lines used were SH-SY5Y (human neuroblastoma cells), HEK293 (human embryonic kidney cell line), HL-1 (cardiac myocyte cell line), and Caco-2 (human intestinal epithelial cell line), which exhibit different levels of ACE2 enzyme expression. An MTT assay was performed on all cell lines after 24 h of treatment. The results showed that IC_{50} values in all tested cell lines were above 40 μM, indicating that compound **4** does not affect cell viability at the tested concentrations (Figure 5 and Table 2).

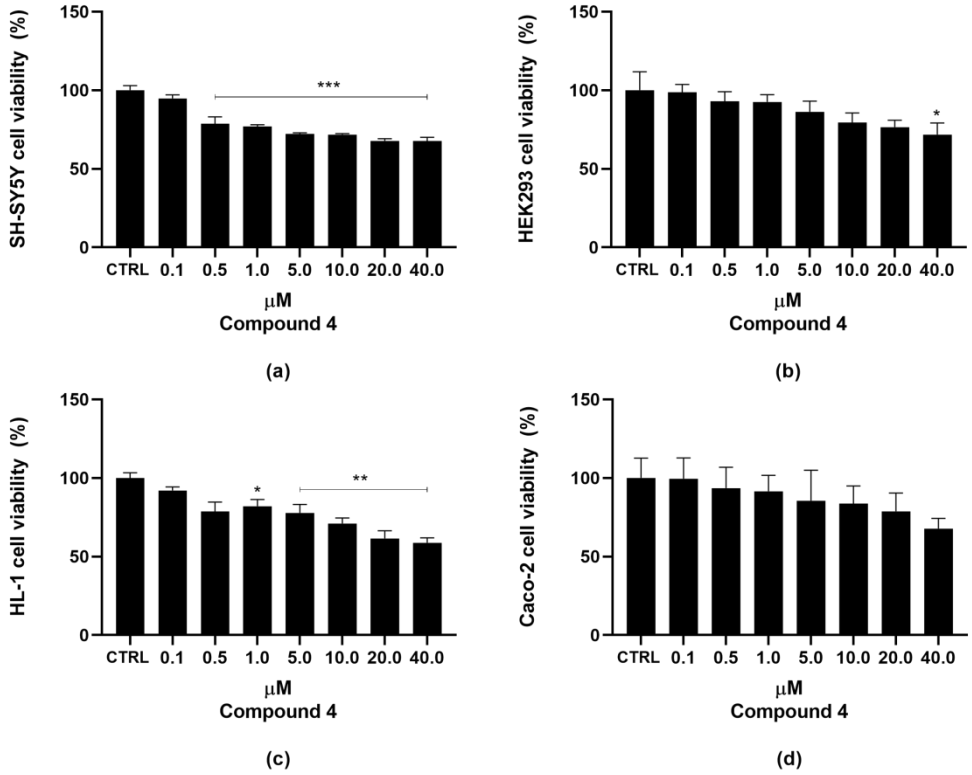

Figure 5. Cell viability assay. SH-SY5Y (**a**), HEK293 (**b**), HL-1 (**c**), and Caco-2 (**d**) cells were exposed to the indicated concentrations of 4 for 24 h, and cell survival was measured using the MTT assay, as described in the Materials and Methods section. The percentage of viable cells was calculated as the ratio between treated and control cells. Vehicle-treated cells were used as the negative control (CTRL). Data are expressed as mean ± standard error (SE) of three replicates from three independent experiments. Statistical significance was evaluated (GraphPad Prism 8.4.2 software) using one-way ANOVA followed by Dunnett's post hoc test. Significance: (* $p < 0.05$, ** $p < 0.01$, *** $p < 0.001$).

Table 2. Summary table of IC_{50} values in SH-SY5Y, HEK293, HL-1, and Caco-2 cell lines.

Cell Line	IC_{50} (μm) Compound 4
SH-SY5Y	>>40 μM
Hek293	

HL-1	
Caco-2	

3.4. Molecular Docking of 1–5 in the Active Site of ACE2

Docking studies were performed with a crystal structure of ACE2 in the conformation inhibited by MLN-4760. The docking procedure involved a search in conformational space with flexibility in the rotamers of the ligand and binding pocket side chains. The highest ranking docking solution displayed a binding of **4** in the ACE2 binding pocket, with an estimated binding energy of −8.4 kcal/mol (Figure 6a). In this docking solution, **4** makes a hydrogen bond with E375 and other interactions with F274, H345, T347, D367, F504, Y510, Y515 and Zn^{2+}. The residues H345, Y515 and Zn^{2+} have been shown to be part of the active site of ACE2 [24]. In the top docking solution, a large part of **4** occupies the same space as MLN-4760 deep into the binding pocket between the two movable domains of ACE2 (Figure 6a and b). In addition, compounds **1**, **2**, **3** and **5** were also docked into the ACE2 structure using the same parameters for compound **4**. Compared with compound **4**, none of the top ranking docking solutions of these other compounds occupied the same space as MLN-4760 close to the active site residues and all of them had lower estimated binding energy (−7.9, −8.3, −8.0 and −7.9 kcal/mol for compound **1**, **2**, **3** and **5**, respectively) (Figure 6c). In conclusion, the docking results suggest that compound **4** is compatible with ACE2 binding and inhibition; furthermore, they provide insight into the potential interactions formed between the inhibitor and the active site residues.

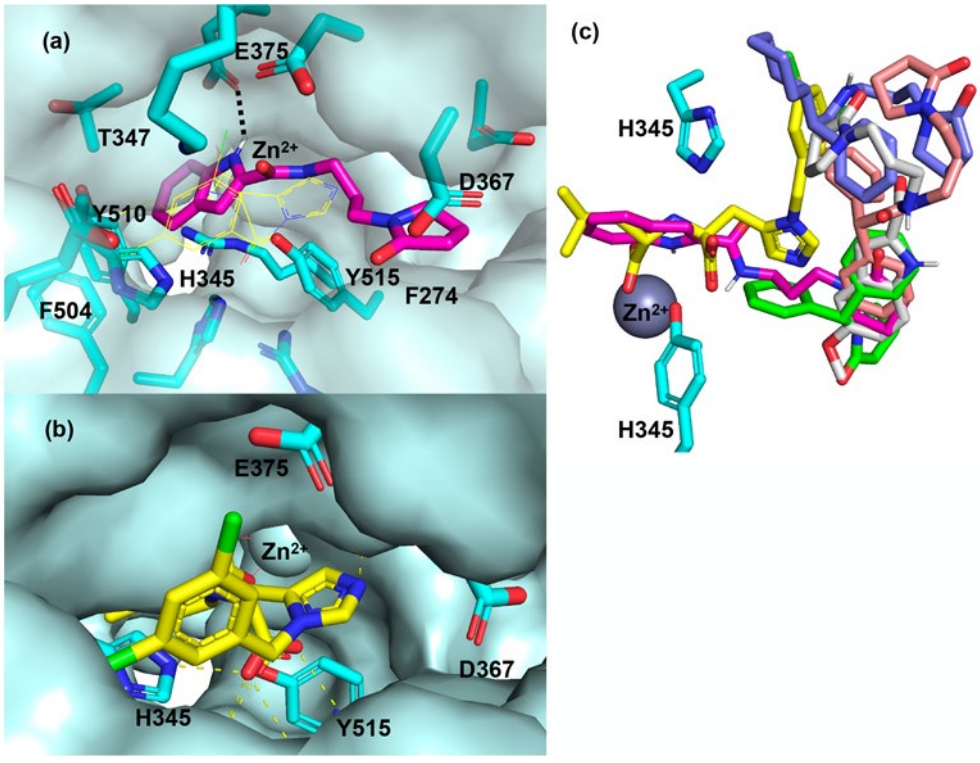

Figure 6. Docking result of compound **4** in the X-ray structure of human ACE2 (**a**). In the active site of ACE2, flexible residues are displayed with sticks and carbons in cyan, and those interacting with **4** are labeled. MLN4760 (**b**) and compounds **1**, **2**, **3** and **5** (**c**) in the active site of ACE2 for comparison. The carbons of compounds **1**, **2**, **3**, **4**, **5** and MLN-4760 are shown in green, salmon, violet, magenta, gray and yellow, respectively.

4. Conclusions

The novel COVID-19 continues to endanger human health, and the therapeutic drugs for its treatment are under intensive research and development. Identifying the efficacy and toxicity of new molecules *in vitro* and *in vivo* models is essential for finding new medications, and a prerequisite for drugs to enter clinical trials. The combination of *in vitro* research techniques with computer simulation methods may lead to the discovery of a new lead compound. *The in vitro* results obtained from our designed and synthesized compounds have identified several potential ACE2 receptor inhibitors. These molecules will now proceed to *in vivo* testing to evaluate their efficacy and safety profiles. These compounds may be used for treating conditions such as pulmonary hypertension, asthma and arterial hypertension. In addition, considering the pivotal role of ACE2 in endothelial function and pathological angiogenesis, the modulation of ACE2 activity may also have broader implications in vascular homeostasis and diseases associated with aberrant angiogenic processes. Although there is no strong evidence that ACE2 receptor inhibitors, such as MLN-4760, can influence the binding with the SARS-CoV-2 spike protein directly [37], it cannot be excluded that they may affect cellular internalization of the virus receptor complex or ACE2 availability on the cell membrane through effects on its expression and turn-over. Therefore, we believe that compound **4**, which inhibits ACE2 (as shown here) and is structurally related to Arbidol (inhibitor of the binding between SARS-CoV-2 spike protein and ACE2), could serve as a lead compound for the future development of therapeutic options for both viral infections and respiratory diseases.

Author Contributions: Conceptualization, C.S. and M.F.A.; methodology, A.C., I.N., and M.M.; software A.V. and F.F.; validation, H.E.-K. and C.S.; formal analysis, A.V. and A.C.; investigation, I.N. and A.C.; resources, M.F.A. and F.G.; data curation, A.V. and I.N.; writing—original draft preparation, F.G., A.C., I.N., and M.M.; writing—review and editing, A.V., A.C., and H.E.-K.; visualization, M.F.A.; supervision, C.S., M.M., and H.E.-K. All authors have read and agreed to the published version of the manuscript.

Funding: This research received no external funding.

Institutional Review Board Statement: Not applicable.

Informed Consent Statement: Not applicable.

Data Availability Statement: Data are contained within the article.

Conflicts of Interest: No conflicts of interest are declared.

References

1. Chen, Y.; Chen, L.; Deng, Q.; Zhang, G.; Wu, K.; Ni, L.; Yang, Y.; Liu, B.; Wang, W.; Wei, C.; et al. The presence of SARS-CoV-2 RNA in the feces of COVID-19 patients. *J. Med. Virol.* **2020**, *92*, 833–840.
2. Chan, J.F.W.; Kok, K.H.; Zhu, Z.; Chu, H.; To, K.K.W.; Yuan, S.; Yuen, K.Y. Genomic characterization of the 2019 novel human-pathogenic coronavirus isolated from a patient with atypical pneumonia after visiting Wuhan. *Emerg. Microb. Infect.* **2020**, *9*, 221–236.
3. Hoffmann, M.; Kleine-Weber, H.; Schroeder, S.; Krüger, N.; Herrler, T.; Erichsen, S.; Schiergens, T.S.; Herrler, G.; Wu, N.H.; Nitsche, A.; et al. SARS-CoV 2 cell entry depends on ACE2 and TMPRSS2 and is blocked by a clinically proven protease inhibitor. *Cell* **2020**, *181*, 271–280.
4. Hamming, I.; Timens, W.; Bulthuis, M.L.C.; Lely, A.T.; Navis, G.V.; van Goor, H. Tissue distribution of ACE2 protein, the functional receptor for SARS coronavirus. A first step in understanding SARS pathogenesis. *J. Pathol.* **2004**, *203*, 631–637.
5. Wu, F.; Zhao, S.; Yu, B.; Chen, Y.M.; Wang, W.; Song, Z.G.; Hu, Y.; Tao, Z.W.; Tian, J.H.; Pei, Y.Y.; et al. A new coronavirus associated with human respiratory disease in China. *Nature* **2020**, *579*, 265–269.

6. Barile, E.; Baggio, C.; Gambini, L.; Shiryaev, S.A.; Strongin, A.Y.; Pellecchia, M. Potential therapeutic targeting of coronavirus spike glycoprotein priming. *Molecules* **2020**, *25*, 2424.
7. Oudit, G.Y.; Crackower, M.A.; Backx, P.H.; Penninger, J.M. The Role of ACE2 in Cardiovascular Physiology. *Trends Cardiovasc. Med.* **2003**, *13*, 93–101. https://doi.org/10.1016/S1050-1738(02)00233-5.
8. Benndorf, R.; Böger, R.H.; Ergün, S.; Steenpass, A.; Wieland, T. Angiotensin II Type 2 Receptor Inhibits Vascular Endothelial Growth Factor–Induced Migration and In Vitro Tube Formation of Human Endothelial Cells. *Circ. Res.* **2003**, *93*, 437–447. https://doi.org/10.1161/01.RES.0000088358.99466.04.
9. Zhang, Q.; Sihong, L.; Li, T.; Yu, L.; Zhang, Y.; Zeng, H.; Qian, X.; Bi, J.; Lin, Y. ACE2 Inhibits Breast Cancer Angiogenesis via Suppressing the VEGFA/VEGFR2/ERK Pathway. *J. Exp. Clin. Cancer Res.* **2019**, *38*, 173. https://doi.org/10.1186/s13046-019-1156-5.
10. Feng, Y.; Ni, L.; Wan, H.; Fan, L.; Fei, X.; Ma, Q.; Gao, B.; Xiang, Y.; Che, J.; Li, Q. Overexpression of ACE2 Produces Antitumor Effects via Inhibition of Angiogenesis and Tumor Cell Invasion In Vivo and In Vitro. *Oncol. Rep.* **2011**, *26*, 1157–1164. https://doi.org/10.3892/or.2011.1394.
11. Shirato, K.; Kawase, M.; Matsuyama, S. Wild-type human coronaviruses prefer cell-surface TMPRSS2 to endosomal cathepsins for cell entry. *Virology* **2018**, *517*, 9–15.
12. Caruso, A.; Tommonaro, G.; Vassallo, A.; Paris, D.; Monné, M.; Catalano, A.; Sinicropi, M.S.; Saturnino, C. Imino and Thioureidic derivatives as new tools for Alzheimer's disease: Preliminary studies. *Chem. Biol. Drug Des.* **2025**, *105*, e70049.
13. Bonomo, M.G.; Caruso, A.; El-Kashef, H.; Salzano, G.; Sinicropi, M.S.; Saturnino, C. An update of carbazole treatment strategies for COVID-19 infection. *Appl. Sci.* **2023**, *13*, 1522.
14. Artusi, S.; Ruggiero, E.; Nadai, M.; Tosoni, B.; Perrone, R.; Ferino, A.; Zanin, I.; Xodo, L.; Flamand, L.; Richter, S.N. Antiviral activity of the G-quadruplex ligand TMPyP4 against herpes simplex virus-1. *Viruses* **2021**, *13*, 196.
15. Isaac-Lam, M.F. Molecular modeling of the interaction of ligands with ACE2–SARS-CoV-2 spike protein complex. *Silico pharmacol.* **2021**, *9*, 55.
16. Caruso, A.; Caira, V.; El-Kashef, H.; Saturnino, C. The potential of indole alkaloids in bone health and osteoporosis management. *Appl. Sci.* **2024**, *14*, 8124.
17. Iacopetta, D.; Catalano, A.; Ceramella, J.; Barbarossa, A.; Carocci, A.; Fazio, A.; La Torre, C.; Caruso, A.; Ponassi, M.; Rosano, C.; et al. Synthesis, anticancer and antioxidant properties of new indole and pyranoindole derivatives. *Bioorg. Chem.* **2020**, *105*, 104440.
18. Sinicropi, M.S.; Caruso, A.; Conforti, F.; Marrelli, M.; Kashef, H.E.; Lancelot, J.C.; Rault, S.; Statti, G.A.; Menichini, F. Synthesis, inhibition of NO production and antiproliferative activities of some indole derivatives. *J. Enzyme Inhib. Med. Chem.* **2009**, *24*, 1148–1153.
19. Caruso, A.; Barbarossa, A.; Carocci, A.; Salzano, G.; Sinicropi, M.S.; Saturnino, C. Carbazole derivatives as STAT inhibitors: An overview. *Appl. Sci.* **2021**, *11*, 6192.
20. Caruso, A. Special Issue "Carbazole Derivatives: Latest Advances and Prospects". *Appl. Sci.* **2023**, *13*, 4263.
21. Grande, F.; De Bartolo, A.; Occhiuzzi, M.A.; Caruso, A.; Rocca, C.; Pasqua, T.; Carocci, A.; Rago, V.; Angelone, T.; Sinicropi, M.S. Carbazole and simplified derivatives: Novel tools toward β-adrenergic receptors targeting. *Appl. Sci.* **2021**, *11*, 5486.
22. Todisco, S.; Infantino, V.; Caruso, A.; Santarsiero, A.; Convertini, P.; El-Kashef, H.; Giuzio, F.; Sinicropi, M.S.; Saturnino, C. Heterocyclic Nitrogen Compounds as Potential PDE4B Inhibitors in Activated Macrophages. *Appl. Sci.* **2024**, *14*, 6747.
23. Choudhary, S.; Silakari, O. Scaffold morphing of arbidol (umifenovir) in search of multi-targeting therapy halting the interaction of SARS-CoV-2 with ACE2 and other proteases involved in COVID-19. *Virus Res.* **2020**, *289*, 198146.
24. Girgis, A.S.; Panda, S.S.; Kariuki, B.M.; Bekheit, M.S.; Barghash, R.F.; Aboshouk, D.R. Indole-based compounds as potential drug candidates for SARS-CoV-2. *Molecules* **2023**, *28*, 6603.
25. Towler, P.; Staker, B.; Prasad, S.G.; Menon, S.; Tang, J.; Parsons, T.; Ryan, D.; Fisher, M.; Williams, D.; Dales, N.A.; et al. ACE2 X-ray structures reveal a large hinge-bending motion important for inhibitor binding and catalysis. *J. Biol. Chem.* **2004**, *279*, 17996–18007.
26. Trott, O.; Olson, A.J. AutoDock Vina: Improving the speed and accuracy of docking with a new scoring function, efficient optimization, and multithreading. *J. Comput. Chem.* **2010**, *31*, 455–461.
27. Souza, U.J.B.D.; Spilki, F.R.; Tanuri, A.; Roehe, P.M.; Campos, F.S. Two years of SARS-CoV-2 Omicron Genomic evolution in Brazil (2022–2024): Subvariant Tracking and Assessment of Regional Sequencing Efforts. *Viruses* **2025**, *17*, 64.
28. Hoffmann, M.; Kleine-Weber, H.; Pöhlmann, S. A multibasic cleavage site in the spike protein of SARS-CoV-2 is essential for infection of human lung cells. *Mol. Cell* **2020**, *78*, 779–784.

29. Glowacka, I.; Bertram, S.; Müller, M.A.; Allen, P.; Soilleux, E.; Pfefferle, S.; Steffen, I.; Tsegaye, T.S.; He, Y.; Gnirss, K.; et al. Evidence that TMPRSS2 activates the severe acute respiratory syndrome coronavirus spike protein for membrane fusion and reduces viral control by the humoral immune response. *J. Virol.* **2011**, *85*, 4122–4134.
30. Fukihara, J.; Kondoh, Y. COVID-19 and interstitial lung diseases: A multifaceted look at the relationship between the two diseases. *Respir. Investig.* **2023**, *61*, 601–617.
31. Ahmad, I.; Pawara, R.; Surana, S.; Patel, H. The repurposed ACE2 inhibitors: SARS-CoV-2 entry blockers of Covid-19. *Top. Curr. Chem*. **2021**, *379*, 40.
32. Nami, B.; Ghanaeian, A.; Ghanaeian, K.; Nami, N.; Ghasemi-Dizgah, A.; Caluseriu, O. The interaction of the severe acute respiratory syndrome coronavirus 2 spike protein with drug-inhibited angiotensin converting enzyme 2 studied by molecular dynamics simulation. *J. Hypertens*. **2021**, *39*, 1705–1716.
33. Wang, X.; Cao, R.; Zhang, H.; Liu, J.; Xu, M.; Hu, H.; Li, Y.; Zhao, L.; Li, W.; Sun, X.; et al. The antiinfluenza virus drug, arbidol is an efficient inhibitor of SARS-CoV-2 in vitro. *Cell Discov.* **2020**, *6*, 28.
34. Padhi, A.; Seal, A.; Tripathi, T. How does Arbidol Inhibit the Novel Coronavirus SARS-CoV-2. Atomistic insights from molecular dynamics simulations. *ChemRxiv* **2020**. https://doi.org/10.26434/chemrxiv.12464576.v1.
35. Jasenovec, T.; Radosinska, D.; Kollarova, M.; Balis, P.; Dayar, E.; Bernatova, I.; Zorad, S.; Vrbjar, N.; Cacanyova, S.; Radosinska, J. Angiotensin system modulations in spontaneously hypertensive rats and consequences on erythrocyte properties; action of MLN-4760 and zofenopril. *Biomedicines* **2021**, *9*, 1902.
36. Benitez Cardoza, C.G.; Vique-Sanchez, J.L. Potential inhibitors of the interaction between ACE2 and SARS-CoV-2 (RBD), to develop a drug. *Life Sci.* **2020**, *256*, 117970.
37. Nami, B.; Ghanaeian, A.; Ghanaeian, K.; Nami, N. The effect of ACE2 inhibitor MLN-4760 on the interaction of SARS-CoV-2 spike protein with human ACE2: A molecular dynamics study. *ChemRxiv* **2020**. https://doi.org/10.26434/chemrxiv.12159945.v1.